4-1-2006

Multistable solitons in the cubic-quintic discrete nonlinear Schrödinger equation

R. Carretero-González
Computational Science Research Center

J. D. Talley
Computational Science Research Center

C. Chong
Computational Science Research Center

B. A. Malomed
Tel Aviv University

Available online at www.sciencedirect.com
SCIENCE DIRECT
Physica D 216 (2006) 77–89
PHYSICA D
www.elsevier.com/locate/physd

Multistable solitons in the cubic–quintic discrete nonlinear Schrödinger equation

R. Carretero-González[a,*], J.D. Talley[a], C. Chong[a], B. . Malomed[b]

[a] *Nonlinear Dynamical Systems Group, Computational Science Research Center and Department of Mathematics and Statistics, San Diego State University, San Diego, C 92182-7720, US* [1]

[b] *Department of Interdisciplinary Studies, Faculty of Engineering, Tel viv University, Tel viv 69978, Israel*

vailable online 3 March 2006

bstract

We analyze the existence and stability of localized solutions in the one-dimensional discrete nonlinear Schrödinger (DNLS) equation with a combination of competing self-focusing cubic and defocusing quintic onsite nonlinearities. We produce a stability diagram for different families of soliton solutions that suggests the (co)existence of infinitely many branches of stable localized solutions. Bifurcations that occur with an increase in the coupling constant are studied in a numerical form. variational approximation is developed for accurate prediction of the most fundamental and next-order solitons, together with their bifurcations. Salient properties of the model, which distinguish it from the well-known cubic DNLS equation, are the existence of two different types of symmetric solitons and stable asymmetric soliton solutions that are found in narrow regions of the parameter space. The asymmetric solutions appear from and disappear back into the symmetric ones via loops of forward and backward pitchfork bifurcations.

Keywords: Nonlinear Schrödinger equation; Solitons; Bifurcations; Nonlinear lattices

1. Introduction

Discrete nonlinear Schrödinger (DNLS) equations constitute an important class of lattice models that are of great interest in their own right [1], and also find direct applications to the description of arrays of waveguides in nonlinear optics, as predicted in Ref. [2], and for the first time realized experimentally in Ref. [3], which used a set of parallel semiconductor waveguides made on a common substrate (see review article Ref. [4] and further references therein). In optics, quasi-discrete waveguide arrays can also be created as virtual photonic lattices in photorefractive materials (see review Ref. [5] and references therein), and can be described approximately by the DNLS equations. The waveguide arrays may support both spatial solitons [3,4] and quasi-discrete spatiotemporal collapse [6].

Besides nonlinear optics, the DNLS model also describes a Bose–Einstein condensate trapped in a strong optical lattice (sinusoidal potential acting on atoms in the condensate), as predicted theoretically [7] and observed experimentally [8] (see also the recent review [9]). dditionally, DNLS equations may be derived naturally, in the rotating-phase approximation, from various nonlinear-lattice models that give rise to discrete breathers (alias intrinsic localized modes); see theoretical papers Refs. [10] and [11] and the first reports on the experimental making of these breathers in Ref. [12].

Properties of discrete solitons in the DNLS equation with the simplest cubic nonlinearity have been studied in detail, including three dimensional settings [13], and are now well understood. These solitons were observed experimentally in arrays of nonlinear optical waveguides [3,4]. They also correspond, in the DNLS approximation, to the intrinsic localized modes in more sophisticated dynamical lattices.

Nonlinear Schrödinger (NLS) equations with more complex nonlinearities were studied in detail in continuum models. s well as their cubic counterparts, such models are of interest

* Corresponding author.
E-mail address: carreter@sciences.sdsu.edu (R. Carretero-González).
URL: http://www.rohan.sdsu.edu/~carreter (R. Carretero-González).
[1] *URL*: http://nlds.sdsu.edu.

0167-2789/$ - see front matter © 2006 Elsevier B.V. ll rights reserved.
doi:10.1016/j.physd.2006.01.022

by themselves, and may also have direct applications [14]. In particular, glasses and organic optical media whose dielectric response features the cubic–quintic (CQ) nonlinearity, i.e., a self-defocusing quintic correction to the self-focusing cubic Kerr effect, are known [15]. Properties of solitons in the NLS equations with the CQ nonlinearity may be very different from those in the simplest cubic equation, especially in the case when the higher-order nonlinearity is combined with a periodic potential. Recently, a great variety of multistable solitons with different numbers of peaks and different symmetries (even, odd, etc.) have been found in the CQ NLS equation embedded in the linear potential of Kronig–Penney (KP) type (a periodic array of rectangular potential wells) [16], after bistable solitons were studied in the CQ NLS equation with a single rectangular potential well [17]. Solitons in the continuum cubic NLS equation with the KP potential have been studied too [18].

The limiting case of the CQ NLS equation with a very strong KP potential naturally reduces to the DNLS equation with the CQ nonlinearity, and our objective in this paper is to construct solitons in this discrete model and explore their stability. The model is not only interesting by itself (as shown in the present work), but may also be realized experimentally in the form of an array of waveguides built of the above-mentioned optical materials featuring the CQ nonlinearity [15]. It is relevant to mention that stable discrete solitons were recently found in the DNLS equation with saturable nonlinearity [20,21] (note that the latter model was introduced back in 1975 by Vinetskii and Kukhtarev [22]), and, moreover, optical discrete solitons supported by the saturable self-defocusing nonlinearity were created experimentally using the photovoltaic effect in a waveguiding lattice built into a photorefractive crystal [23]. We show in this work that discrete solitons in the CQ model are very different from their counterparts investigated in the aforementioned works [20,21,23] (most importantly, they feature a great multistability, as shown below) due to the fundamental fact that, unlike the saturable nonlinearity, the combination of the CQ terms features *competition* of self-focusing and defocusing nonlinearities. For the same reason, the solitons in the CQ DNLS equation are drastically different from ones investigated earlier [24,25] in the DNLS equation with a *single* nonlinear term of an arbitrary power (for instance, quintic instead of cubic). Finally, a quantum version of a finite-length DNLS equation (Bose–Hubbard model) with the CQ nonlinearity and periodic boundary conditions was considered in Ref. [26], where states with a small number q of quanta (in most cases, $q \leq 6$) were constructed.

The manuscript is organized as follows. In the next section, we introduce the model and its stationary solutions, and derive a two-dimensional map to generate discrete solitons corresponding to homoclinic solutions. Section 3 reports various (multistable) soliton solutions and their stability. In Section 4, we focus on bifurcations that create/annihilate different solutions and account for the exchange of stability between them. In Section 5, we present an analytical variational approximation that correctly predicts the main bifurcation branches. Section 6 concludes the paper.

2. The model and dynamical reductions

The one-dimensional cubic–quintic discrete nonlinear Schrödinger (CQ DNLS) equation is

$$\mathrm{i}\dot{\psi}_n + C\quad \psi_n + B|\psi_n|^2\psi_n \quad Q|\psi_n|^4\psi_n = 0, \tag{1}$$

where ψ_n are the complex fields at site n (in the case of the above-mentioned array of optical waveguides, ψ_n is the amplitude of the electromagnetic wave in the given core), $\dot{\psi} \equiv \mathrm{d}\psi/\mathrm{d}t$ (in the above-mentioned model of the waveguide array, the evolutional variable is actually not time but the coordinate along the waveguide), and the discrete second derivative (discrete-diffraction operator in the array of waveguides) is $C\quad \psi_n \equiv C(\psi_{n+1} + \psi_{n\ 1}\quad 2\psi_n)$, where C is the constant of the tunnel coupling between the cores. The third and fourth terms in Eq. (1) represent, respectively, the cubic and quintic nonlinearities. We assume that $C, B, Q > 0$, which (as said above) corresponds to the most natural case of the self-focusing cubic (Kerr) nonlinearity competing with its self-defocusing quintic counterpart. Upon renormalization of ψ and t, we set $B = 2$ and $Q = 1$.

Eq. (1) conserves two dynamical invariants: the Hamiltonian,

$$H = \sum_n \left[C\psi_n^*(\psi_{n+1} + \psi_{n\ 1}\quad 2\psi_n) + |\psi_n|^4\quad \frac{1}{3}|\psi_n|^6 \right], \tag{2}$$

and norm,

$$M = \sum_n |\psi_n|^2 \tag{3}$$

(in the application to the optical waveguide array, the latter is the total power of the light signal).

We aim to look for a soliton solution with frequency μ by substituting

$$\psi_n = u_n \exp(\ \mathrm{i}\mu t) \tag{4}$$

in Eq. (1). The real stationary lattice field u_n must solve the equation

$$\mu u_n + C(u_{n+1} + u_{n\ 1}\quad 2u_n) + 2u_n^3\quad u_n^5 = 0, \tag{5}$$

supplemented by the condition of the vanishing of u_n at $n \to \pm\infty$, i.e., the soliton can be looked for as a *homoclinic solution* of Eq. (5) (an alternative approach would be to use an algebraic method of Ref. [27]). Note that stationary soliton solutions of Eq. (5) depend on two parameters, μ and C.

We will study soliton solutions and their stability by viewing Eq. (5) as a recurrence relation between consecutive amplitudes, which can be cast in the form of a two-dimensional map,

$$\begin{cases} u_{n+1} &= au_n \quad v_n \quad 2C\ {}^1u_n^3 + C\ {}^1u_n^5 \\ v_{n+1} &= u_n, \end{cases} \tag{6}$$

where $a \equiv 2\quad \mu/C$. Constant solutions to Eq. (1) correspond to fixed points (FPs) of this map. There exists at most five

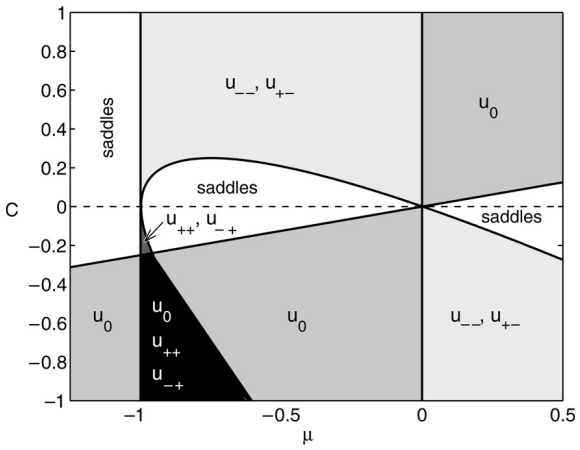

Fig. 1. Stability diagram for the fixed points (FPs) of the two-dimensional map (6). In non-shaded areas, all the FPs are saddles. Shaded areas represent regions where the indicated FPs are centers. The diagonal line and the tilted parabola correspond, respectively, to $C = \mu/4$ and $(C + 1 + \mu)^2 = 1 + \mu$.

FPs, which we arrange in increasing order and label as $u_{--}, u_{+-}, u_0, u_{-+}, u_{++}$, with $u_0 = 0$ and

$$u_{\pm\pm} = \pm\sqrt{1 \pm \sqrt{1+\mu}}. \tag{7}$$

The stability of all the FPs within the framework of map (6) can easily be derived from the linearization of the map around these FPs, leading to the stability chart displayed in Fig. 1.

In this framework, soliton solutions correspond to homoclinic orbits connecting the FP at origin ($u_0 = 0$) with itself, in the case when it is a saddle. The FP $u_0 = 0$ is a saddle for $\{\mu < 0, C > \mu/4\}$ and for $\{\mu > 0, C < \mu/4\}$. We are only interested in physically meaningful couplings, so we restrict our attention to $C > 0$. Furthermore, the regions for $\mu < -1$ and $\mu > 0$ produce stable and unstable manifolds that do not intersect each other. Therefore, in the remainder of this work, we restrict our area of interest to $C > 0$ with $-1 < \mu < 0$.

In Fig. 2, we depict a progression of the homoclinic tangles (webs of such orbits) emanating from the saddle points as the coupling constant C increases. For small C, the homoclinic-connection structure is very rich, including many orbits (i.e., many soliton solutions). As C increases, many connections disappear through a series of bifurcations (see below), so that a single homoclinic loop survives at very large C, which corresponds to the well-known exact soliton solution of the continuum CQ NLS equation [28].

Note that, in contrast to the cubic DNLS equation, the CQ discrete equation gives rise to a pair of extra fixed points that support heteroclinic orbits (as shown in Fig. 2). The detailed

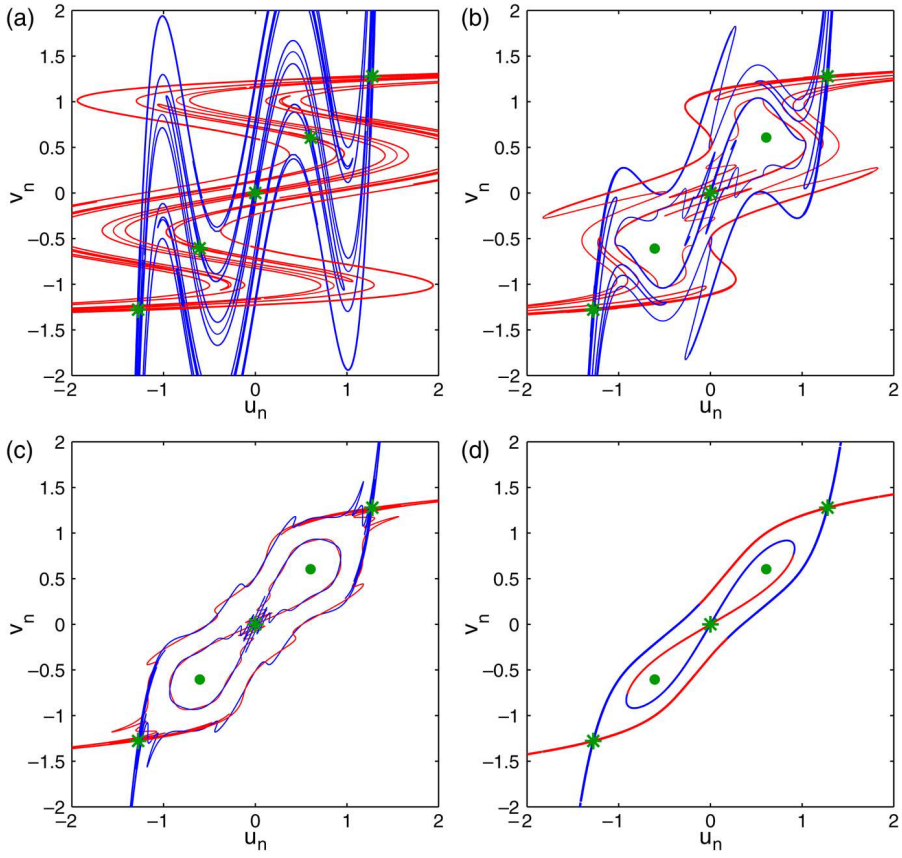

Fig. 2. Homoclinic tangles generating localized solutions of Eq. (1) for $\mu = -0.6$, with the coupling constant C increasing from left to right and from top to bottom: (a) $C = 0.15$, (b) $C = 0.4$, (c) $C = 0.8$, and (d) $C = 2$. Saddle points and centers are designated by asterisks and circles, respectively. For small C, the homoclinic intersections have a much richer structure, including homoclinic and heteroclinic connections between all five fixed points. For large C, only one homoclinic and one heteroclinic solution survive (together with their $u_n \leftrightarrow -u_n$ symmetric counterparts).

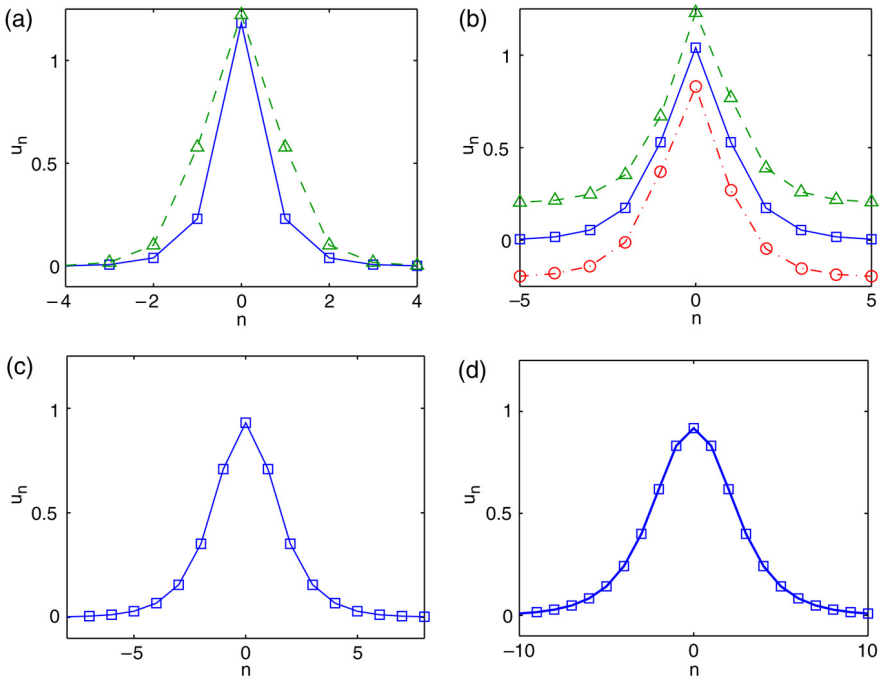

Fig. 3. Typical examples of soliton solutions generated by the homoclinic tangles of Fig. 2 as the coupling parameter C increases. Insets pertain to the same values of parameters as the corresponding insets in Fig. 2. (a) Pair of coexisting symmetric solution for small C. (b) s C increases, only one stable symmetric solution exists (squares), together with a pair of asymmetric solutions (triangles and circles) appearing in small regions of the parameter space (the asymmetric solutions have been displaced vertically for clarity of presentation). (c) Further increase in C destroys all stable solutions except for the symmetric one which, as seen in panel (d), tends towards the continuum soliton in the limit of $C \to \infty$. The parameters are $\mu =$ 0.6 and (a) $C = 0.15$, (b) $C = 0.4$, (c) $C = 0.8$, and (d) $C = 2$.

study of these heteroclinic orbits, which correspond to dark solitons or kinks, falls outside the scope of this work. Here we concentrate on the homoclinic orbits and (bright) soliton solutions corresponding to them.

In Fig. 3 we depict a selection of typical solitons corresponding to the homoclinic tangles in Fig. 2. Each solution is generated numerically by taking the soliton shape as predicted in an approximate form by the homoclinic intersections, and then applying a Newton-type algorithm to find a numerically exact localized solution of Eq. (5). In panel (a), we show a couple of solitons coexisting at given parameter values. Panel (b) depicts a triplet of coexisting solutions that form part of a loop of pitchfork bifurcations responsible for the creation of *asymmetric* solutions (see below). Finally, panels (c) and (d) show the unique site-centered (the maximum of the soliton is located at a single central site, cf. Fig. 5(a)) solution which survives in the continuum limit, $C \to \infty$.

3. Multistability of discrete solitons

We now aim to explore the structure of the homoclinic tangles and their bifurcations in detail by varying the parameters μ and C. s mentioned previously, for small C the rich homoclinic structure leads to the coexistence of multiple solitons at the same values of μ and C, which is a distinctive feature of the CQ model with the competing nonlinearities: in the cubic DNLS equations, this variety of solitons is not observed [1]. Principal types of the localized solutions for small C (taking $C = 0.1$ as an example) are depicted in Fig. 4. The following scheme is adopted to denote different species of the solitons. The solution generated by the first (main) homoclinic crossing of the stable and unstable manifolds of the origin (see Fig. 4(a)) is denoted by S_1. This family corresponds to site-centered solitons, the label S standing for *short*, as the solitons of this type correspond to the shortest family of homoclinic crossings. s C is increased, the S_1 soliton suffers a series of alternating stability switches (bifurcations). We use the notation S_k to denote solitons corresponding to the series of *stable* regions between the stability switches. In this work we do not consider higher-order crossings corresponding to repeated iterates in both the stable and unstable manifolds, which would produce *bound states* of the discrete solitons, alias multi-humped or multi-breather (non-fundamental) solutions [29].

The solitons generated by the homoclinic crossings in Fig. 4(b)–(d) correspond, in our notation, to T_1, T_2 and T_3 solitons, T standing for *tall* solitons. They are generated by the second family of crossings, and are characterized by a higher soliton maximum, in comparison with their S counterparts.

The subscript in the notation for the T_k and S_k solutions also helps to differentiate between *site-centered* solutions, for k odd, and *bond-centered* (alias *intersite-centered*) solutions for even k, which feature two central sites with equal magnitude; see examples in Fig. 5.

The S_1, T_1, T_2 and T_3 solitons generated by the highlighted crossings in Fig. 4 are all *stable* solutions. The stability was checked by calculating the respective eigenvalues from Eq. (1) linearized around the stationary solutions, and also verified by direct numerical integration of the full equation (1) after adding a random perturbation to the soliton with a (rather large) relative amplitude of 5%. The evolution of the perturbed solutions is

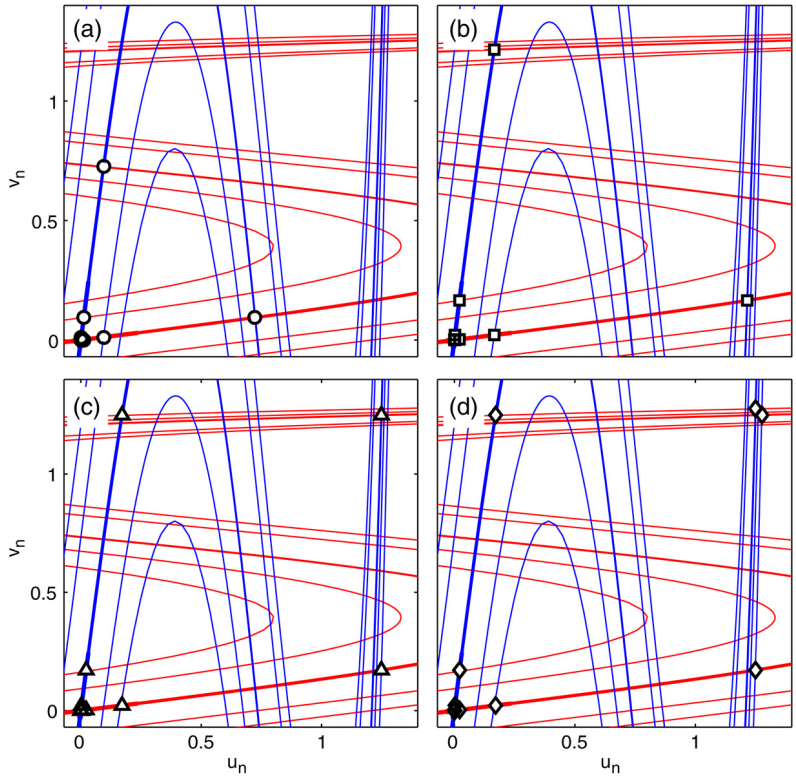

Fig. 4. Multistability of discrete solitons in the CQ DNLS equation is illustrated by displaying the homoclinic tangles generating *stable* localized solutions (see Fig. 5). Parameters are $\mu = 0.6$ and $C = 0.1$ (which corresponds to the point marked by the asterisk in the T_1 region in Fig. 6). Panels (a), (b), (c) and (d) correspond, respectively, to the discrete solitons of the S_1, T_1, T_2, and T_3 types (see definitions in the text).

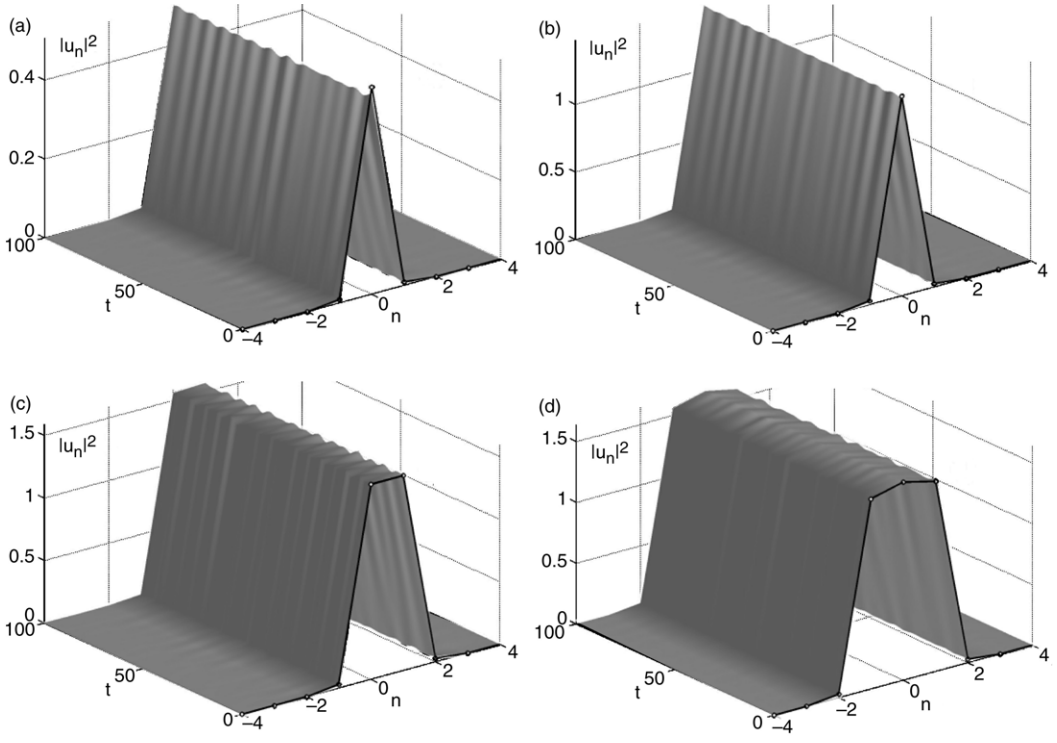

Fig. 5. Evolution of the solitons generated by the homoclinic intersections depicted in Fig. 4 after adding random perturbations, with a relative amplitude of 5%, to the initial configuration (dark line).

displayed in Fig. 5, where the unperturbed solitons are shown by dark lines for $t = 0$. The perturbed solutions oscillate about the unperturbed solitons, confirming their stability (the oscillations do not fade, because the system is conservative).

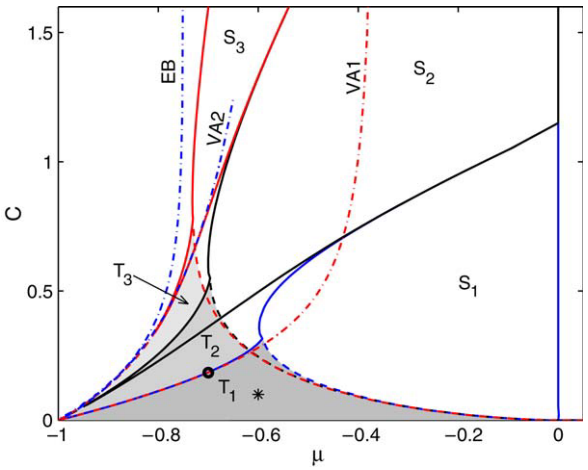

Fig. 6. The stability diagram for single-hump localized solitons of the cubic–quintic discrete NLS equation (1). Note that each S_k region has a "wedge" that penetrates into the corresponding T_k region. The existence region of the solitons is bounded by the curve EB, at which the homoclinic connections of the origin disappear. The curves V 1 and V 2 show the variational approximations described in Section 5. more detailed description is given in the text.

In order to identify a stability region of the soliton family in the (μ, C) parameter plane, we start with a particular soliton solution of S or T type, generated as described above, and then continue it by varying the parameters, simultaneously computing the stability eigenvalues. The continuation procedure started at small C where, as said above, it is easy to find a particular solution.

The resulting stability diagram for the solitons of $S_{1,2,3}$ and $T_{1,2,3}$ types is displayed in Fig. 6. The T_k-stable regions (shaded in Fig. 6) feature a tent-like shape, with the base on the line $C = 0$ with $1 \leq \mu \leq 0$. Since all these regions share the common base, there should be a nontrivial area where, presumably, the T_k solitons exist and are *stable for all values of* k. It is also apparent from the stability diagram in Fig. 6 that the stability regions for the S_k solutions with different k, in contrast to their T_k counterparts, do not intersect each other. Therefore, solitons of S type feature no multistability.

We note that each S_k stability region features a wedge that penetrates into the region of stability of the T_k solitons. In particular, the T_1 region is completely embedded in the S_1 region. This property suggests that, for any k, there always exist non-empty regions where the T_k and S_k solitons coexist and are *simultaneously stable*. It is interesting too that the S-stability regions outlive their T counterparts as C increases. This is due to the fact that the T solutions correspond to the second family of homoclinic crossings that disappear, in saddle-node bifurcations (see below), earlier than the first family of crossings (i.e., the S solutions).

Existence regions for the solitons, which may be broader than the regions where the solitons are stable, are defined as those in which the stable and unstable manifolds emanating from the origin do intersect. We have computed such a region numerically. In Fig. 6, it is located to the right of the dashed–dotted line EB (*existence boundary*). To the left of this curve, no localized solutions are possible. s C increases, the EB curve approaches the line $\mu = 3/4$, which corresponds to the existence border for solitons in the continuum limit of the CQ equation [16]. More specifically, the existence regions of the T solutions *exactly coincide* with their stability regions, i.e., the solitons of T type are *always stable*. The existence region for the S solutions has a complex structure, contained in the region where homoclinic connections exist to the right of the EB curve, while the stability area for these solitons is *really smaller* than the existence region. We also note that (as explained in detail below) the S_k solutions represent only two distinct families of solitons, one site-centered (for odd k) and one bond-centered (for even k).

Since some solitons of the S type are unstable, it is necessary to determine what the instability transforms them into. s an example, in the top row of Fig. 7 we display the evolution of an unstable S_2 soliton in the stability region of T_1 (for $(\mu, C) = (\ 0.6, 0.15)$, see the asterisk in Fig. 6), together with its instability eigenvalues. The nonlinear evolution proceeds through periodic oscillations between two asymmetric states (see the dashed lines for $t = 0$).

In the bottom row of Fig. 7 we show the evolution of another unstable solution and its associated instability spectrum. In this case, we take the S_1 solution at $(\mu, C) = (\ 0.6, 0.4)$, which is in the gap between the stability regions of the S_1 and S_2 solutions. *loop* of pitchfork bifurcations occurs in the gaps between consecutive S-stability regions; see details in the next section. The evolution of this unstable solution amounts to periodic oscillations between the original S_1 soliton (the solid line at $t = 0$) and its translation by one site (the dashed line at $t = 0$). Therefore, this solution is a time-periodic one, being close to a heteroclinic connection linking the two unstable solutions, S_1 and its translation.

4. Bifurcations of the discrete solitons

In this section we aim to explain how the T_1 solutions disappear and how the evolution of the S solutions leads to stability changes and the creation of pairs of *stable asymmetric* solitons. It is straightforward to understand the simultaneous disappearance of the S- and T-type solutions as C increases. The boundary on which this happens corresponds to the left side of the tent-like stability area of the T solutions in Fig. 6. The S_k and T_k solutions collide on this boundary and disappear in a saddle-node bifurcation. This bifurcation can easily be followed using the homoclinic-tangle approach (see Fig. 8). Before the bifurcation occurs, i.e., below the boundary (see the asterisk in Fig. 6), two intersections, identified by squares and triangles in Fig. 8(a), generate the solitons of types S_1 and T_1, respectively, which are shown in the left panels of Fig. 11. In contrast, when the bifurcation curve is approached, see Fig. 8(b), the stable and unstable manifolds barely intersect, and the two solitons are nearly identical. Exactly at the bifurcation, the manifolds touch tangentially, and only one solution is generated (i.e., the S_1 and T_1 solitons are identical at this point). fter this saddle-node bifurcation, these solutions do not exist anymore.

nother family of noteworthy bifurcation points corresponds to cuspidal points of the T-stability regions. Three types

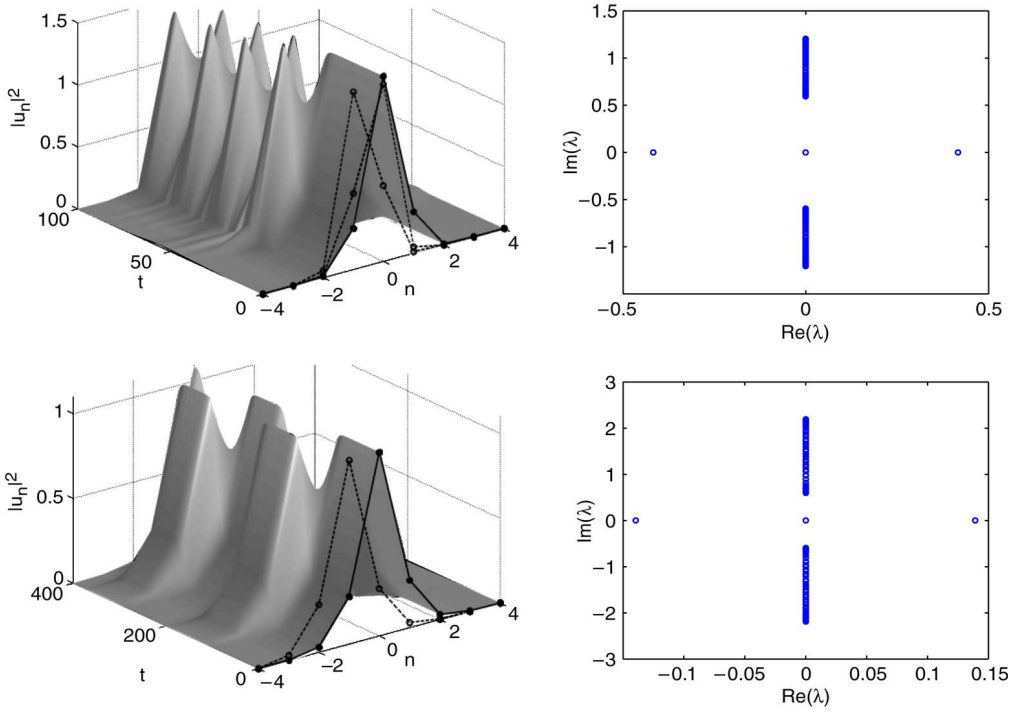

Fig. 7. Evolution of unstable solitons (left panels), together with their instability spectrum (right panels). The top row depicts the evolution of an unstable S_2 soliton, shown by the dashed line in Fig. 3(a) for $(\mu, C) = (\ \ 0.6, 0.15)$, initiated by a small perturbation. fter some transient, the initial configuration (solid line) evolves to one featuring oscillations between two asymmetric states (dashed lines). The bottom row depicts the evolution of an unstable symmetric S_1 solution from Fig. 3(b) for $(\mu, C) = (\ \ 0.6, 0.4)$. The evolution amounts to oscillations between the initial configuration (solid line) and its translation by one site (dashed line). The respective (in)stability spectra for the two solutions in the left column are depicted in the right column.

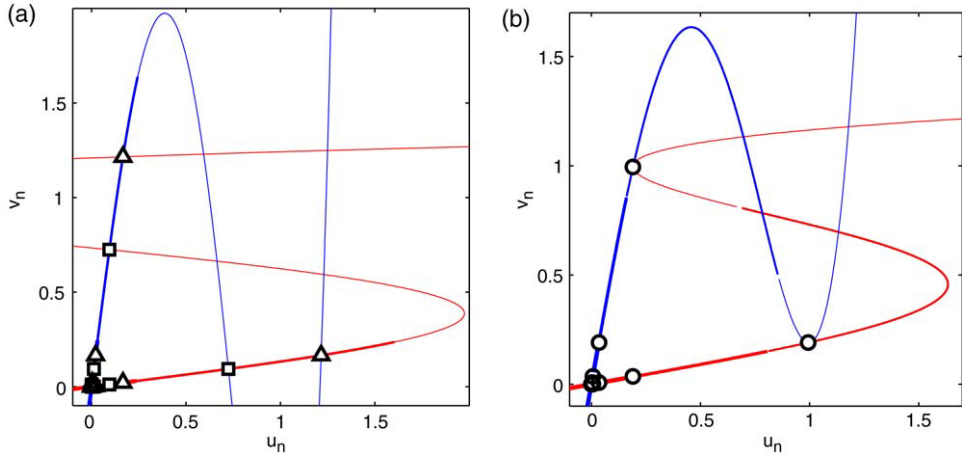

Fig. 8. Homoclinic tangles generating the solitons in Fig. 11. (a) The point $(\mu, C) = (\ \ 0.6, 0.1)$ belongs to the bistability region (see asterisk in Fig. 6) which generates two solitons (triangles, T_1, and squares, S_1). (b) The point $(\mu, C) = (\ \ 0.7, 0.1855)$ is located on the bifurcation curve (see the circle in Fig. 6), hence the two solutions collapse into one (see the right panel in Fig. 11).

of bifurcations occur near these points: ( ) the saddle-node bifurcation described above, at which the S and T solitons collide and disappear; (B) another saddle-node bifurcation, at which the T solutions disappear; and (C) a bifurcation at which the S solitons lose their stability. These bifurcations are depicted in Fig. 9 as follows: ( ) corresponds to going through panels (f) → (e) → (b), (B) is displayed by a chain of panels (f) → (g) → (d), and (C) corresponds to going through (d) → (a) → (b).

Bifurcation (C) deserves more attention. In Fig. 10, we depict in more detail the bifurcation scenario corresponding to a route from the stability region of S_1 to its S_2 counterpart, which passes through a gap where no S solution is stable. Panels (a) through (g) show the homoclinic tangles as C increases, for fixed $\mu =$ 0.55. Parameter values for each of these panels are indicated in panel (h) and its magnification in panel (i). From this figure, the existence of a pitchfork loop — a supercritical pitchfork shortly followed by an inverted supercritical pitchfork — is evident. In panel (a), we depict by a square point one

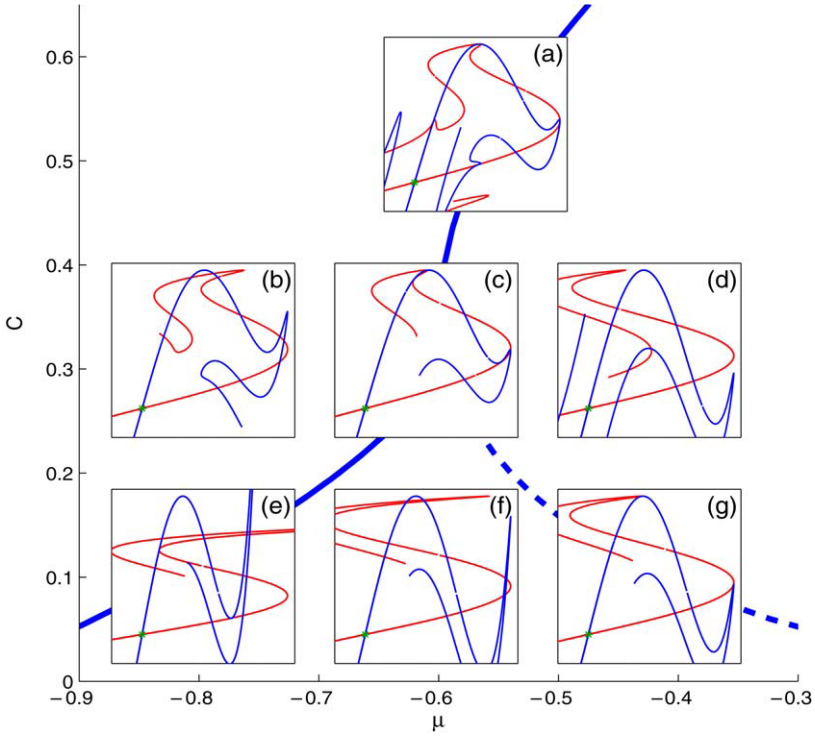

Fig. 9. Different types of bifurcations around the cusp of the T_1 region. saddle-node bifurcation corresponding to panel (e) annihilates the pair of the S_1 and T_1 solutions (the same bifurcation was depicted in Fig. 8). nother saddle-node bifurcation corresponds to panel (g) and is responsible for the destruction of the T_1 solution. Going from (d) to (a), there is a pitchfork bifurcation which is responsible for the loss of stability of the symmetric soliton and the creation of a pair of stable asymmetric solitons (see further details in Fig. 10).

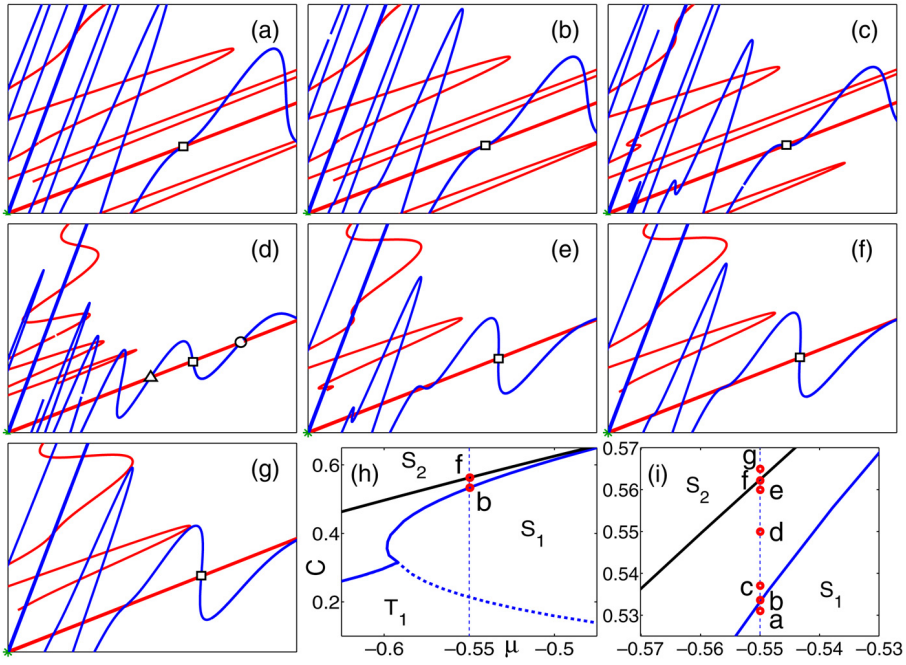

Fig. 10. The pitchfork bifurcation leading to asymmetric soliton solutions. This series of plots was obtained by keeping $\mu =$ 0.55 and varying C from the S_1 to S_2 regions, as shown in insets (h) and (i). The series includes the following panels: (a) the S_1 region before the bifurcation; (b) at the pitchfork bifurcation; (c), (d) and (e) in the region where asymmetric solitons exist; (f) is a *reverse pitchfork* that destroys the asymmetric solutions; and (g) the S_2 region after the latter bifurcation. The square dot represents the same homoclinic orbit throughout the bifurcation, while the triangle and circle in (d) correspond to the asymmetric solitons from Fig. 3.

of the homoclinic intersections, which gives rise to solution S_1. s C increases, the supercritical pitchfork bifurcation is reached, panel (b), which gives rise to a pair of extra homoclinic intersections (see panel (c) and the triangle and circle in panel

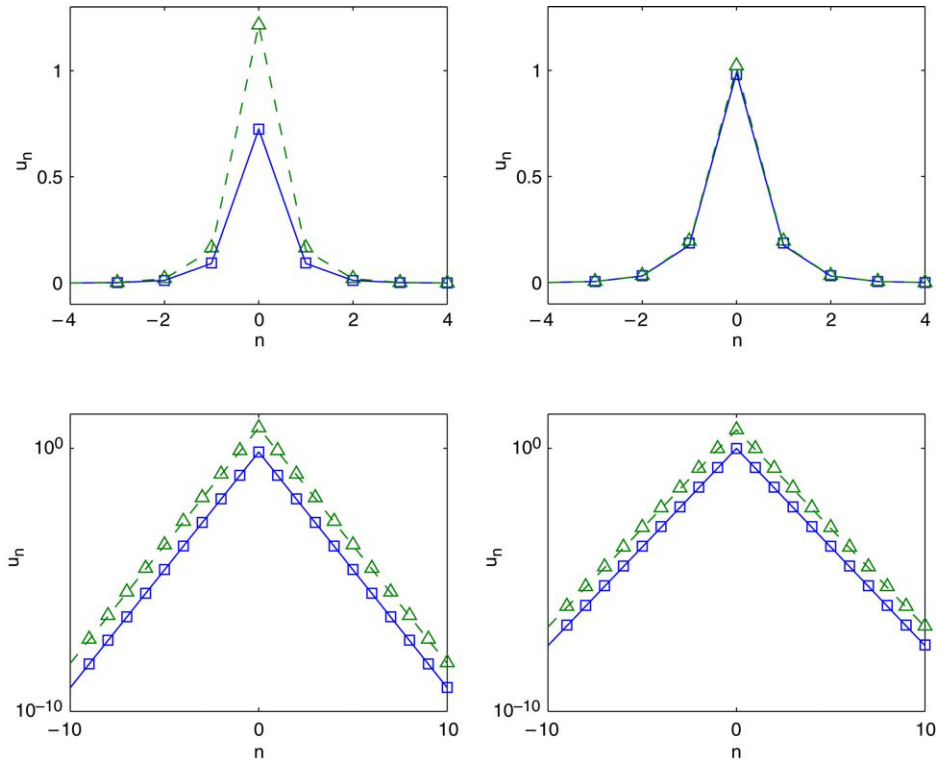

Fig. 11. Soliton solutions of Eq. (5) for $(\mu, C) = (\ \ 0.6, 0.1)$ (left) and $(\mu, C) = (\ \ 0.7, 0.1845)$ (right) are shown on straight (top) and logarithmic (bottom) scales. Points and lines correspond, respectively, to numerically exact solutions and solutions predicted by the variational approximation. The right panels correspond to a point (μ, C) close to the collision of the soliton solutions of S_1 and T_1 types (see the circle in Fig. 6).

(d)). s C increases further, the reverse subcritical pitchfork occurs, eliminating the extra pair of intersections.

Quite interesting are the shape and stability of solitons that this extra pair generates in the narrow gap between the S_k and S_{k+1} stability regions (which coincides with the region of the pitchfork loop), where these new solutions exist. They represent *asymmetric* solitons of the CQ DNLS equation, which are depicted in Fig. 3(b) by means of triangles and circles. s might be expected, the stability is swapped by the pitchfork bifurcations. Indeed, the S solitons are unstable inside the pitchfork loop, where the new asymmetric solutions are *stable*. n example of unstable evolution of an S soliton inside the pitchfork loop is shown in the bottom row of Fig. 7. We stress that such pitchfork loops, and the respective asymmetric solitons, do not exist in the cubic DNLS equation (asymmetric solitons were also found in a DNLS equation with a mixture of cubic onsite and intersite nonlinearities [19]).

Further inspection of the pitchfork loop demonstrates that, if the S_1 *site-centered* soliton looses its stability through the direct bifurcation, then the reverse bifurcation, which closes the loop, stabilizes an S_2 *bond-centered* soliton. t the next pitchfork loop (in the gap between the stability of S_2 and S_3), the latter bond-centered solution loses its stability and, after the loop, an S_3 *site-centered* soliton gains its stability. s C is increased further, this process repeats itself, creating stability bands for the S_k solitons for larger k. In fact, all the solutions S_k represent only two distinct soliton families emanating from the principal homoclinic intersection: site-centered solutions and bond-centered solutions; the pitchfork loops conducting stability swaps between the two families. For a given S_k, the number of the pitchfork loops passed by the soliton, while developing from the anti-continuum ($C = 0$) limit, is $k \quad 1$.

The existence of *stable* bond-centered solitons is a noteworthy feature by itself as, in the usual DNLS model with cubic nonlinearity, only site-centered states are stable (in the DNLS equation with the saturable onsite nonlinearity, stable bond-centered solitons were found too [20]). n interesting issue that still has to be addressed is if there exists an accumulation curve for the pitchfork loops, or if the loops continue to appear as one approaches the continuum limit, $C \to \infty$.

5. The variational approximation

The variational approximation (V) can be used to describe the shape of stationary soliton solutions in an analytical form. The method will not only be successful in approximating the shape of the most fundamental solitons, but will also predict the saddle-node bifurcation where the T_1 and S_1 solutions collide and disappear.

The only tractable *ansatz* for the V in the discrete models is one based on an exponential cusp, which was applied in Ref. [25] to solitons in the above-mentioned DNLS equation with an arbitrary power nonlinearity:

$$u_n = \quad \mathrm{e} \quad ^{|n|}, \tag{8}$$

with real positive constants and . We identify the value of without resorting to the V proper, but rather from the

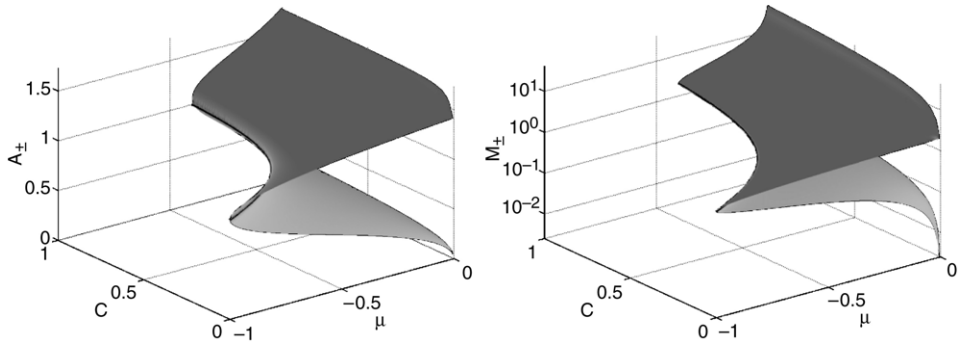

Fig. 12. mplitude (left) and norm M (right) for the two soliton solutions predicted by the V (the scale for the norm is logarithmic). The top and bottom branches correspond to the tall and short solitons, respectively. The dark solid line represent the bifurcation curve where the two solutions are predicted to coalesce and disappear.

substitution of ansatz (8) in Eq. (5) linearized for the decaying tail of the soliton, which yields

$$= \ln\left(\frac{a}{2} + \sqrt{\left(\frac{a}{2}\right)^2 \quad 1}\right) \tag{9}$$

(recall that $a \equiv 2 \quad \mu/C$). Thus, a necessary (but not sufficient) condition for the existence of any soliton solution is $a > 2$, or $\mu < 0$ (since we set $C > 0$, it will then guarantee that Eq. (9) yields a real positive). We stress that the latter soliton-existence condition is an *exact* one, as it follows from the straightforward consideration of the exponentially localized tails of the soliton, and does not exploit any approximation.

Now we invoke the V proper, treating the amplitude in ansatz (8) as a variational parameter, while was already fixed as per Eq. (9) (i.e., by the condition that the ansatz must match the correct asymptotic form of the soliton solution).

The stationary equation (5) can be derived from the Lagrangian

$$L = \sum_{n=\ \infty}^{\infty}\left[\mu u_n^2 + \frac{B}{2}u_n^4 \quad \frac{Q}{3}u_n^6 \quad C(u_{n+1} \quad u_n)^2\right]. \tag{10}$$

Substitution of the ansatz into the Lagrangian and explicit calculation of the sum lead to the following effective Lagrangian, which is the main ingredient of the V [30]:

$$L_{\text{eff}}(\ ) = \mu \ ^2\coth(\ ) + \ ^4\coth(2 \ ) \\ \frac{6}{3}\coth(3 \ ) \quad 2\tanh(\ /2)C \ ^2. \tag{11}$$

Then the Euler–Lagrange equation, $\mathrm{d}L_{\text{eff}}(\ )/\mathrm{d} \ = 0$, yields a quadratic equation for ^{2}:

$$\coth(3 \ ) \quad ^2\Big)^2 + 2\coth(2 \ ) \quad ^2\Big) \\ + \mu\coth(\ ) \quad 2\tanh(\ /2)C = 0. \tag{12}$$

Eq. (12) indicates that there may be two different solutions. The top panel of Fig. 12 depicts the amplitude associated with these two solutions predicted by the V . It is clear that the two solutions coalesce and disappear at the bifurcation curve (solid line). In Fig. 11 we display examples of these two variational solutions, together with the solutions obtained numerically from Eq. (5) through Newton iterations. It is observed that the match between the numerical and variational solutions is extremely good for small values of the coupling parameter C. For larger values of C, the solution tends to its continuum (smooth) analogue, where the cusp-shaped ansatz (8) is obviously irrelevant.

The V predicts the bistable solutions of the type (8) inside the (μ, C)-parameter regions where the quadratic equation (12) admits two distinct positive roots. The comparison with numerical results in Fig. 11 immediately shows that the two different variational solutions exactly correspond to the S_1 and T_1 solitons, as they were defined above. Therefore, the curve where Eq. (12) has a double root represents the saddle-node collision of S_1 and T_1. This bifurcation curve predicted by the V is depicted by the dashed–dotted curve labeled V 1 in Fig. 6. It is quite remarkable that the approximation based on the simple ansatz (8) is able to capture the saddle-node bifurcation so well for small C.

It is possible to refine the V approach by allowing a more general ansatz of the form

$$u_n = \begin{cases} \mathrm{e} \quad ^{|n|} & \text{if } |n| > 0, \\ \beta & \text{if } n = 0, \end{cases} \tag{13}$$

where we introduce a new free parameter β. This new ansatz is able to predict the existence of the solitons of two distinct types, which can be immediately identified with short (S) and tall (T) solitons, which were described in detail above.

The new variational ansatz (13), with two independent variational parameters (, β), is able to very accurately predict the whole existence region of the T_1 solution, as well as the saddle-node bifurcation that creates the S_3 solution. The boundary of the S_3 solitons predicted by the improved V is depicted by the dash–dotted line V 2 in Fig. 6. s seen from the figure, the new V gives an extremely good approximation for the boundary, up to C 1. The results for the existence region of the T_1 soliton predicted by this V are not depicted in Fig. 6 because they exactly coincide (up to the resolution of the figure) with *both* left and right numerically found boundaries for the T_1 soliton; see the darker shaded area in Fig. 6 (the simple V , based on ansatz (8), which gives rise to curve V 1, only captured the left boundary).

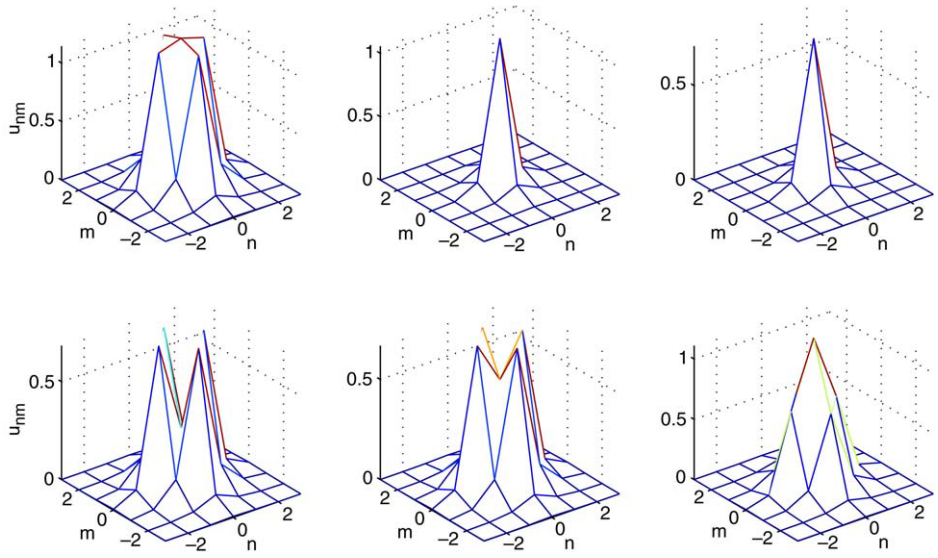

Fig. 13. Two-dimensional coexisting soliton solutions for $(\mu, C) = (\ 0.6, 0.07)$. The top row depicts three coexisting *stable* soliton solutions, while the bottom row represents three coexisting *unstable* soliton solutions. ll these solutions were obtained by Newton iteration on the steady-state equation with initial seeds predicted by the two-dimensional variational approximation with ansatz (14).

The improved V with ansatz (13) is also able to pick up solutions with a dip at the central site, corresponding to $\beta <$ e in the ansatz, i.e., a bound state of two solitons, or "multi-breathers" [29]. Thus, the modified V is able to describe the respective bifurcation curves too (the results are not presented here).

well-known approach to predicting the stability for soliton families is based on the Vakhitov–Kolokolov (VK) criterion [31]. The VK criterion states that a solution family, parameterized by the frequency μ, as in Eq. (4), may be stable if $\mathrm{d}M/\mathrm{d}\mu < 0$, and is definitely unstable otherwise, where M is the soliton's norm defined as per Eq. (3). The simplest variational ansatz (8) yields $M = \ ^2 \coth(\ )$ (note that both and depend on (μ, C) through Eqs. (9) and (12)). The norm given by the latter expression is depicted, as a function of (μ, C), in the right panel of Fig. 12. It is clear from the figure that $\mathrm{d}M/\mathrm{d}\mu > 0$ for the T_1 soliton, and $\mathrm{d}M/\mathrm{d}\mu < 0$ for S_1 (these results can be proven analytically, within the framework of the V). Thus, the VK criterion suggests that the T_1 soliton is unstable, while its S_1 counterpart may be stable. Comparing this conclusion with the numerical results for the stability reported above, we conclude that the VK criterion *does not* apply to our model. In fact, similar conclusions for the failure of the VK criterion were obtained in the *continuous* CQ NLS equation with an external potential, which might be both a single rectangular potential well [17] and a periodic lattice of rectangular wells (the above-mentioned Kronig–Penney potential) [16].

natural question that arises is the existence of multistable solutions in higher-dimensional lattices. The higher-dimensional equivalent of (1) is obtained by replacing the one-dimensional index n and the discrete Laplacian by their higher-dimensional analogues. Unfortunately, the homoclinic approach is not applicable in higher-dimensional lattices. Nonetheless, the variational approach presented here is still amenable in the higher-dimensional case. Namely, a natural ansatz equivalent to (13), but now in two dimensions (2D), becomes

$$u_{nm} = \begin{cases} \mathrm{e}^{\ (|n|+|m|)} & \text{if } |n| + |m| > 0, \\ \beta & \text{if } n = m = 0, \end{cases} \tag{14}$$

where now we have two indices (m, n) along the two spatial dimensions, and the decay is the same as for the one-dimensional case (cf. Eq. (9)). Preliminary results indicate the coexistence of *stable* soliton solutions in the 2D model. s an example, in Fig. 13 we depict six coexisting solutions for the same parameter values. The top row in the figure depicts three *stable* coexisting solutions. It is worth mentioning that the variational approach for the 2D case is also able to capture other solutions, such as stable and unstable multi-humped profiles (see the bottom row of Fig. 13). detailed stability analysis for higher-dimensional (2D and 3D) soliton solutions falls outside the scope of the present paper and will be presented elsewhere.

6. Conclusions and extensions

The objective of this work was to introduce the discrete nonlinear Schrödinger (DNLS) equation with the competing cubic–quintic (CQ) nonlinearities. Besides being a new dynamical model, it may also apply to the description of an array of optical waveguides with the intrinsic CQ nonlinearity.

We have studied the multistability of discrete solitons in the model, looking for homoclinic solutions to the respective stationary discrete equation. Regions of the existence and stability of single-humped soliton solutions were identified by using a numerical continuation method based on Newton-type iterations. The stability of the various types of the solitons was investigated through numerical evaluation of eigenvalues for small perturbations. The resulting stability diagram suggests the existence of an infinite family of branches of *stable* solitons

of the aforementioned type T_k, for sufficiently small values of the coupling constant C. s C increases, these solutions get destroyed through saddle-node bifurcations. We have also identified another type of discrete soliton solutions, S_k, with S_{odd} surviving in the continuum limit, $C \to \infty$. The stability of solutions of the latter type (S) changes, with the increase of C, through a series of small pitchfork loops (each opens with a supercritical pitchfork, which is shortly followed by a reverse supercritical pitchfork). Inside the loops, the symmetric solitons S_k lose their stability, while a pair of *stable asymmetric* solutions is created. The latter solutions have no counterpart in the cubic DNLS equation, nor in the continuum CQ NLS equation. Finally, using the variational approximation (V), we were able to approximate the main branches of the solutions and their bifurcations for small C. We have also proposed an improved version of the V , with two free parameters rather than one, that drastically (qualitatively) upgrades the accuracy of the V , making it possible to predict simultaneously the most fundamental solitons and some higher-order ones.

n interesting extension of this work would be to thoroughly investigate localized solutions in the two-dimensional version of the CQ DNLS equation, which may be realized, for instance, as a *bunch* of the corresponding nonlinear optical waveguides (cf. the recently reported experimental realization for linear waveguides [32]). In particular, the existence and stability of *asymmetric* solitons in the two-dimensional model would be an issue of great interest. nother promising direction for further consideration may be the study of kink solutions, corresponding to heteroclinic trajectories generated by the intersection of the stable and unstable manifolds of different fixed points of the map (6).

s concerns the underlying mathematical theory, an intriguing issue is to understand why the Vakhitov–Kolokolov criterion was found to fail consistently in the discrete CQ NLS equation and its counterpart with a periodic potential in the continuum case [16,17].

cknowledgments

We appreciate valuable discussions with J. Fujioka and . Espinosa. B. .M. appreciates the hospitality of the Institute of Physics at the Universidad Nacional utónoma de México, and the Nonlinear Dynamical Systems group[2] at the Department of Mathematics and Statistics, San Diego State University (SDSU). This author was partially supported by a Window-on-Science grant provided by the European Office of erospace Research and Development of the US ir Force. R.C.G. and C.C. acknowledge the Grant-in- id award provided by the SDSU Foundation. R.C.G. also acknowledges support from NSF-DMS-0505663. J.D.T. is grateful for the support of the Computational Science Research Center[3] at SDSU.

References

[1] P.G. Kevrekidis, K.Ø. Rasmussen, .R. Bishop, Internat. J. Modern Phys. B 15 (2001) 2833.
[2] D.N. Christodoulides, R.I. Joseph, Opt. Lett. 13 (1988) 794.
[3] H.S. Eisenberg, Y. Silberberg, R. Morandotti, .R. Boyd, J.S. itchison, Phys. Rev. Lett. 81 (1998) 3383.
[4] D.N. Christodoulides, F. Lederer, Y. Silberberg, Nature 424 (2003) 817.
[5] J.W. Fleischer, G. Bartal, O. Cohen, T. Schwartz, O. Manela, B. Freedman, M. Segev, H. Buljan, N.K. Efremidis, Opt. Express 13 (2005) 1780.
[6] D. Cheskis, S. Bar- d, R. Morandotti, J.S. itchison, H.S. Eisenberg, Y. Silberberg, D. Ross, Phys. Rev. Lett. 91 (2003) 223901.
[7] . Trombettoni, . Smerzi, Phys. Rev. Lett. 86 (2001) 2353;
G.L. lfimov, P.G. Kevrekidis, V.V. Konotop, M. Salerno, Phys. Rev. E 66 (2002) 046608;
R. Carretero-González, K. Promislow, Phys. Rev. 66 (2002) 033610.
[8] F.S. Cataliotti, S. Burger, C. Fort, P. Maddaloni, F. Minardi, . Trombettoni, . Smerzi, M. Inguscio, Science 293 (2001) 843;
M. Greiner, O. Mandel, T. Esslinger, T.W. Hänsch, I. Bloch, Nature 415 (2002) 39.
[9] M. . Porter, R. Carretero-Gonzalez, P.G. Kevrekidis, B. . Malomed, Chaos 15 (2005) 015115.
[10] S. ubry, Physica 103D (1997) 201;
R.S. MacKay, S. ubry, Nonlinearity 7 (1994) 1623;
S. Flach, C.R. Willis, Phys. Rep. 295 (1998) 181;
G.P. Tsironis, Chaos 13 (2003) 657.
[11] D.K. Campbell, S. Flach, Y.S. Kivshar, Phys. Today 57 (2004) 43.
[12] M. Sato, B.E. Hubbard, .J. Sievers, B. Ilic, D. . Czaplewski, H.G. Craighead, Phys. Rev. Lett. 90 (2003) 044102;
M. Sato, .J. Sievers, Nature 432 (2004) 486.
[13] R. Carretero-González, P.G. Kevrekidis, B. . Malomed, D.J. Frantzeskakis, Phys. Rev. Lett. 94 (2005) 203901;
P.G. Kevrekidis, B. . Malomed, D.J. Frantzeskakis, R. Carretero-González, Phys. Rev. Lett. 93 (2004) 080403.
[14] T. Dauxois, M. Peyrard, Physics of Solitons, Cambridge University Press, 2005.
[15] F. Smektala, C. Quemard, V. Couderc, . Barthélémy, J. Non-Cryst. Solids 274 (2000) 232;
G. Boudebs, S. Cherukulappurath, H. Leblond, J. Troles, F. Smektala, F. Sanchez, Opt. Commun. 219 (2003) 427;
C. Zhan, D. Zhang, D. Zhu, D. Wang, Y. Li, D. Li, Z. Lu, L. Zhao, Y. Nie, J. Opt. Soc. mer. B 19 (2002) 369.
[16] I.M. Merhasin, B.V. Gisin, R. Driben, B. . Malomed, Phys. Rev. E 71 (2005) 016613;
J. Wang, F. Ye, L. Dong, T. Cai, Y.-P. Li, Phys. Lett. 339 (2005) 74.
[17] B.V. Gisin, R. Driben, B. . Malomed, J. Opt. B: Quant. Semiclass. Opt. 6 (2004) S259.
[18] W.D. Li, . Smerzi, Phys. Rev E 70 (2004) 016605;
B.T. Seaman, L.D. Carr, M.J. Holland, Phys. Rev. 71 (2005) 033622.
[19] M. Öster, M. Johansson, . Eriksson, Phys. Rev. E 67 (2003) 056606.
[20] M. Stepić, D. Kip, L. Hadžievski, . Maluckov, Phys. Rev E 69 (2004) 066618;
L. Hadžievski, . Maluckov, M. Stepić, D. Kip, Phys. Rev. Lett. 93 (2004) 033901.
[21] . Khare, K.Ø. Rasmussen, M.R. Samuelsen, . Saxena, J. Phys. Math. Gen. 38 (2005) 807.
[22] V.O. Vinetskii, N.V. Kukhtarev, Sov. Phys. Solid State 16 (1975) 2414.
[23] F. Chen, M. Stepic, C.E. Ruter, D. Runde, D. Kip, V. Shandarov, O. Manela, M. Segev, Opt. Express 13 (2005) 4314.
[24] E.W. Laedke, K.H. Spatschek, S.K. Turitsyn, Phys. Rev. Lett. 73 (1994) 1055;
S. Flach, K. Kladko, R.S. MacKay, Phys. Rev. Lett. 78 (1997) 1207.
[25] B. . Malomed, M.I. Weinstein, Phys. Lett. 220 (1996) 91.
[26] J. Dorignac, J.C. Eilbeck, M. Salerno, .C. Scott, Phys. Rev. Lett. 93 (2004) 025504.
[27] G.P. Tsironis, J. Phys. : Math. Gen. 35 (2002) 951.
[28] Kh.I. Pushkarov, D.I. Pushkarov, I.V. Tomov, Opt. Quantum. Electron. 11 (1979) 471;
S. Cowan, R.H. Enns, S.S. Rangnekar, S.S. Sanghera, Canad. J. Phys. 64 (1986) 311.

[2] http://nlds.sdsu.edu.
[3] http://www.sci.sdsu.edu/csrc/.

[29] T. Bountis, H.W. Capel, M. Kollmann, J.C. Ross, J.M. Bergamin, J.P. van der Weele, Phys. Lett. 268 (2000) 50;
T. Kapitula, P.G. Kevrekidis, B. . Malomed, Phys. Rev. E 63 (2001) 036604;
V. Koukouloyannis, S. Ichtiaroglou, Phys. Rev. E 66 (2002) 066602;
V. Koukouloyannis, Phys. Rev. E 69 (2004) 046613.
[30] B. . Malomed, Progr. Opt. 43 (2002) 71.
[31] N.G. Vakhitov, . . Kolokolov, Izv. Vyssh. Uchebn. Zaved. Radiofiz. 16 (1973) 10120; Radiophys. Quantum Electron. 16 (1973) 783.
[32] T. Pertsch, U. Peschel, F. Lederer, J. Burghoff, M. Will, S. Nolte, . Tunnermann, Opt. Lett. 29 (2004) 468.